Absence of Evidence of Electrical Switching of the Antiferromagnetic Néel Vector

C. C. Chiang, S. Y. Huang, D. Qu, P. H. Wu, and C. L. Chien

Phys. Rev. Lett. **123**, 227203 — Published 27 November 2019
DOI: 10.1103/PhysRevLett.123.227203

Absence of evidence of electrical switching of antiferromagnetic Néel vector

C. C. Chiang[1], S. Y. Huang[1]*, D. Qu[2], P. H. Wu[1], and C. L. Chien[1,2,3]

[1]Department of Physics, National Taiwan University, Taipei 10617, Taiwan
[2]Institute of Physics, Academia Sinica, Taipei, 11529, Taiwan
[3]Department of Physics and Astronomy, Johns Hopkins University, Baltimore, MD 21218, USA

Abstract

Much theoretical and experimental attention has been focused on electrical switching of antiferromagnetic (AF) Néel vector via spin orbit torque (SOT). Measurements employing multi-terminal patterned structures of Pt/AF show recurring signals of supposedly planar Hall effect and magnetoresistance, implying AF switching. We show in this work that similar signals have been observed in structures with and *without* the AF layer, and of even larger magnitude using different metals and substrates. These may not be the conclusive evidences of SOT switching of AF, but the thermal artifacts of patterned metal structure on substrate. Large currents densities in the metallic devices, beyond the ohmic regime, can generate unintended anisotropic thermal gradients and voltages. AF switching requires unequivocal detection of AF Néel vector before and after SOT switching.

Purely electrical control of magnetic devices is an ultimate goal in spintronics. Previously, spin transfer torque (STT) can provide electrical switching of ferromagnetic (FM) layers but requiring at least two FM entities, e.g., Co/Cu/Co, where the spin-polarized current from one FM switches the magnetization of the other FM [1]. The recent discovery of spin orbit torque (SOT) accommodates electrical switching of a single FM layer adjacent to a heavy metal (HM), such as in HM/FM bilayers [2-4]. SOT switching is based on the spin Hall effect (SHE), where a charge current through the HM (e.g., Pt) with a large spin Hall angle θ_{SH} generates a pure spin current in the lateral direction with the spin index σ in the third direction. Above a threshold current density, the SOT can electrically switch the adjacent FM with in-plane anisotropy as well as perpendicular magnetic anisotropy (PMA), but the latter requires an external field along the current direction, thus highly undesirable. Several schemes have been demonstrated to achieve field-free SOT switching of FM layer with PMA [5-12].

It has been well established in both STT and SOT that switching of the magnetization $\boldsymbol{M}$ of an FM layer occurs *only* when the current density j has exceeded the critical value j_c [1-12]. There is no appreciable change of $\boldsymbol{M}$ at $j < j_c$, regardless of the duration of the current or the number of such current pulses. Only until $j \geq j_c$, swift and irreversible changes in $\boldsymbol{M}$ occur. Switching (or lack thereof) can be readily revealed by the measurement of $\boldsymbol{M}$ using magnetometry, or more simply, by suitable Hall effect and magnetoresistance (MR). The evidences for switching are unequivocal and can be readily verified by rotating $\boldsymbol{M}$ of the FM via a small magnetic field to the specific directions.

The recent proposal of electrical switching via SOT of antiferromagnetic (AF) materials, with the potential of ushering in AF spintronics with THz frequencies, has attracted much attention [13-18]. However, unlike FMs, AFs have no net magnetization ($\boldsymbol{M}$ = 0), weakly responsive to magnetic field, but displaying a rich variety of AF spin structures from uniaxial to Kagome. Most theoretical and experimental studies of AF switching have focused on the simplest AFs with two co-linear sublattice magnetizations in opposite directions $\boldsymbol{M_1} = -\boldsymbol{M_2}$ defining a Néel vector $\boldsymbol{n}_{\text{Néel}} = (\boldsymbol{M_1} - \boldsymbol{M_2})/2M_o$, where M_o is the magnitude of the sublattice magnetization. Theories suggest that the antidamping SOT, but not the field-like SOT, can switch the AF Néel vector $\boldsymbol{n}_{\text{Néel}}$ with $\boldsymbol{M}$ = 0 [19]. However, ascertaining electrical switching of the AF Néel vector remains a formidable challenge, compounded by the fact that most AFs have no well-defined $\boldsymbol{n}_{\text{Néel}}$.

Experimental exploration of AF switching was first reported in epitaxial thin films of CuMnAs, an unusual metallic AF with broken inversion symmetry [13]. As such, it is argued that CuMnAs (a similar situation also exists in Mn_2Au) affords Néel SOT switching without the necessity of an adjacent HM layer [13-15]. Most AF switching studies have used Pt/NiO, where the SOT from Pt may switch NiO [16-18], a well-known AF insulator. It has been assumed in the AF switching studies that the AF thin films would acquire the same AF spin structures as those in bulk crystals, a premise that has not been born out in extensive studies of exchange bias, which also involves AF thin films [20].

To detect AF switching, most studies have employed multi-terminal structures, such as the 4-terminal or the 8-terminal patterned structure. The 8-terminal structure, consisting of four electrical lines oriented at 0°, 45°, 90°, and 135°, is intended to capture the planar Hall effect (PHE) resistance R_{XY} in Fig. 1(a) and the MR resistance R_{XX} in Fig. 1(b) after the large writing current 1 (blue) and 2 (red) (along the 45° or 135° lines) switches the AF Néel vector. The reading current and the measured voltage for both R_{XY} and R_{XX} are marked by I+, I-, V+ and V- in Fig. 1(a) and (b). The MR may be the anisotropic MR (AMR) in metallic AFs [13-15] or the spin Hall MR (SMR) in Pt/AF bilayers [16-18, 21-23]. We used the same patterned 8-terminal structure and obtained the same qualitative results as those in CuMnAs and Mn_2Au without HM, and in Pt/NiO. The crucial questions are whether these are evidences for SOT switching of the AF Néel vector.

We use the *same* Pt(4)/NiO(60) bilayers, where polycrystalline 4 nm Pt and 60 nm NiO bilayers have been made by magnetron sputtering, onto substrate and patterned into the same 8-terminal devices with 20 μm wide writing leads along the 45° and the 135° directions, and 10 μm wide reading leads along the 0° and the 90° directions for R_{XY} and R_{XX}. For example, a writing current of 32 mA through the 20 μm wide Pt (4 nm) gives a current density of 4 x 10^7 A/cm^2. We use pulsed writing currents of magnitude I with the same pulse width of 10 ms. After a 10 s delay time, the resistances R_{XY} and R_{XX} are subsequently measured at a much lower current density of 2.5×10^5 A/cm^2 from the reading leads. Our results of R_{XY} and R_{XX} of Pt(4)/NiO(60)/Si are shown in Fig.1(c) and (d) respectively. They are expressed as the relative changes of Hall resistance ΔR_{XY} and longitudinal resistance ΔR_{XX}, where ΔR_{XY} steadily decreases (increases) with the number of writing current 1 blue (2 red) pulses of 32 mA along the 45° (135°) line, and ΔR_{XX} changes oppositely. The recurring results of ΔR_{XY} and ΔR_{XX} between write current 1 and 2, very similar to those observed in CuMnAs, Pt/NiO, and Mn_2Au, have previously been claimed as evidence of SOT switching of AFs [13-18]. However, these highly unusual results warrant closer analyses.

First of all, the results in Fig. 1(c) and (d) show that each current pulse of writing current 1 (blue) creates essentially the *same incremental* change in ΔR_{XY} and ΔR_{XX}. If these were related to AF switching, it would imply that each current pulse would create a small but similar Néel vector rotation and/or AF domain reversal. The extent of AF switching would scale with the *number* of pulses, i.e., more pulses would cause a larger portion of switching. Reverting to writing current 2 (red), each current pulse would create the *same* but *reversed* incremental change in AF switching. These behaviors, if indeed due to AF switching, would be diametrically different from those known in SOT or STT switching of FM systems, where, at $j < j_c$, there are no incremental change, nor reversed incremental change, nor accumulative changes of magnetization reversal at all [1-12].

It is also important to stress the large writing current of 32 mA with a high current density of 4 x 10^7 A/cm^2 in Fig. 1(c) and 1(d). At I < 25 mA, we obtained only $R_{XY} \approx 0$ and $\Delta R_{XY} \approx 0$; $R_{XX} \approx$ constant and $\Delta R_{XX} \approx 0$. Only with a larger current, e.g., 32 mA, could we measure appreciable R_{XY}, ΔR_{XY} and ΔR_{XX}, the size of which *scales* with the write current I. At a slightly higher current of $I \approx 35$ mA the sample was destroyed. We illustrate these aspects with another nominally the same Pt(4)/NiO(60)/Si sample from low current to the breakdown current using one-shot pulses, as shown in Fig. 2. Below 25 mA, $R_{XY} \approx 0$ and $\Delta R_{XY} \approx 0$; $R_{XX} \approx 90.6\ \Omega$ and $\Delta R_{XY} \approx 0$, and these values are independent of I. This is the ohmic regime, in which the voltage is linearly proportional to current yielding a constant resistance independent of current. Ohmic regime is where resistance measurements of any metal are normally made, with a lower current to avoid excessive joule heating. The results of $R_{XY} \approx 0$ and $\Delta R_{XY} \approx 0$ indicate there is no PHE signal, i.e., no evidence of AF switching.

However, at I > 25 mA, R_{XY} and R_{XX} rise sharply with I, as shown in Fig. 2(a) and 2(c), respectively, i.e., highly non-ohmic, and at 42 mA the device breaks down. Only in the non-ohmic regime with a very high current can one observe the sizable changes for ΔR_{XY} and ΔR_{XX} on pulse writing current with different orientations, as shown in Fig. 2(b). The values of R_{XX}, ΔR_{XX}, R_{XY}, and ΔR_{XY} are not constant but rise sharply with I. Thus, the evidences of AF switching to date, the increasing and decreasing ΔR_{XY}, could just be the results of the resistance measurements in the non-ohmic regime at very high current density, just below the breakdown current. The high current density exceeding 10^7A/cm^2 also develops serious thermal issues with irreversible damages due to intense heat and electromigration. After such high current densities, the resistance of the metallic devise has suffered permanent changes.

Since R_{XY} and R_{XX} are electrical characteristics, one expects the results to be intrinsic to Pt(4)/NiO(60) and independent of the insulating substrate on which the patterned Pt(4)/NiO(60) structures are situated. Quite the contrary, we found both R_{XY} and R_{XX} depend greatly on substrates. The results of the same patterned structures on glass, as shown in Fig. 1(e) and (f), are much larger than those on Si, with those on MgO in between (not shown). This indicates a strong influence of substrate for electrical measurements at very high current density, in particular, the heat dissipation through the substrate. The larger ΔR_{XY} and ΔR_{XX} for structures on glass, as compared to those on Si, are due to the lower thermal conductivity κ of glass as shown in Table I. Therefore, the same structures when patterned on glass substrate exhibit similar signals but of far greater magnitude. Note that the writing current in Pt/NiO/Glass [Fig. 1(e)] is only 8 mA, but the values of ΔR_{XY} are much larger than those for Pt/NiO/Si [Fig. 1(c)] at 32 mA. Likewise, the ΔR_{XX} for Pt/NiO/Glass shown in Fig. 1(f) at 5 mA are much larger than those for Pt/NiO/Si at 32 mA shown in Fig. 1(d). Because of the much lower κ for glass, Pt/NiO/Glass also has a much lower onset current for the non-ohmic regime and breakdown current than those for Pt/NiO/Si. Since only the writing current dictates the strength of the SOT that switches the Néel vector of AF NiO, the large variations in ΔR_{XX}, ΔR_{XY}, and the onset writing current due to different substrates strongly indicate these are not evidences of SOT switching of AF Néel vector.

We further patterned the same 8-terminal structure on Si, MgO, and glass with only the metal Pt and *without* the AF layer of NiO, thus removing any possibility of AF switching. Still, the *same* saw-tooth recurring patterns in ΔR_{XY} and ΔR_{XX} can be observed, as shown in Fig. 3. These signals, without NiO, increase in the order of Pt/Si, Pt/MgO and Pt/Glass, reflecting the thermal conductivity of the substrates, and illustrating that these recurring results are non-ohmic joule heating in Pt only. Thus, the recurring saw-tooth signals in Pt/NiO are unrelated to SOT AF switching.

The 8-terminal devices were designed to exploit planar Hall effect (PHE) and MR to reveal the SOT switching of the AF Néel vector. While PHE and MR are established methods for detecting the direction of ***M*** of the FM layer, they have never been demonstrated for detecting the Néel vector of an AF layer, for there is no simple method to create and orient the AF Néel vector to the specific directions on demand. Unfortunately, the 8-terminal patterned structure also creates unforeseen complications in electrical measurements. The 8 terminals are connected to the *same common* area, which receives the writing current of a large current density and whose electrical characteristics are subsequently measured to assess possible AF switching. The intended PHE and MR results inadvertently include unintended contributions of asymmetrical temperature gradient, thermal voltages, and Hall voltages.

Only a high writing current beyond the ohmic regime, with current density in the 10^7 A/cm^2 range, generates measureable values of R_{XY} and ΔR_{XY}. After the application of a writing current 1 (blue) pulse, there is a large temperature rise in the 45° line, by more than 100 K, as corroborated by the COMSOL simulation as shown in Fig. 4 (a) and (c), which creates a net temperature gradient between the voltage leads in the 90° line. For the R_{XY} measurements, the current and voltage leads are along the 0° and the 90° lines respectively. This leads to the Seebeck effect in the direction of the temperature gradient. Any metal, (e.g., Pt, Cr, and Au) with a significant Seebeck effect gives rise to a thermal voltage with increasing magnitude for each successive writing current 1 (blue) pulse. When one reverts to the writing current 2 (red), the 135° line is now heated. As compare with Fig. 4 (b) and (d), the temperature gradient between the voltage leads in the 90° line now reverses to give an opposite sign of thermal voltage, that increases with each successive writing current pulses. The simulation values are qualitatively consistent with experiments with relative Seebeck coefficient around 8 μV/K [24, 25]. These temperature differences and voltages, scale sharply with current as shown in Fig. 4 (e) and (f), giving the appearance of recurring Hall resistance signals, by the same token, the MR voltage as well, as shown in Supplemental Material Fig. S1 [26]. In addition to Pt, we have also patterned Cr and Au. As shown in Supplemental Material Fig. S2 [26], the signals for Cr are much larger than those of Pt and Au because of the larger Seebeck coefficient of Cr [28]. These thermal voltages, intrinsic to the metal layer of Pt, Au, and Cr, have nothing to do with AF switching.

Previous studies of AF switching have noted the intense heat in the device [29-30]. Some protocols, e.g., a pause of 10 s after the writing current pulse before the electrical measurements, have been used to alleviate the heating problem. Our measurements reveal that 10 s is far too short for the intense heat to dissipate. In fact, we have found a sizable ΔR_{XY} and temperature gradient remains in the patterned structures even after one hour. Very high current density may also anneal the thin films, cause electromigration and other irreversible damages, causing permanent changes of the resistance, as shown in Supplemental Material Fig. S2 [26]. Furthermore, after the sample has been subjected to a high writing current pulse, subsequent measurements at a lower current may reveal saw-tooth of different magnitudes, and in some cases, even altering the saw-tooth shape into step-like signals [31], as illustrated in Supplemental Material Fig. S3 [26]. Recent experiments also indicate non-spin torque origin of AF switching [32].

In summary, much attention has been focused recently on SOT switching of AF Néel vector employing multi-terminal patterned structures that show recurring signals in PHE ΔR_{XY} and MR ΔR_{XX} signals. We show in this work that these voltage and resistance signals may not be conclusive evidence of SOT switching of AF, but the artifacts of the large writing currents beyond the ohmic regime through the metallic multi-terminal devices. The prospect of SOT switching of AF Néel vector encounters numerous challenges. Many AFs have complex spin structures without a well-defined Néel vector. Even for AFs that may accommodate a Néel vector, it remains a challenge to unequivocally detect the AF Néel vector, before and after the SOT switching.

Acknowledgement --This work was supported by the Ministry of Science and Technology of Taiwan, under the Grant MOST 106-2628-M-002-015-MY3. This work was also partially supported by Academia Sinica and National Taiwan University. We thank D. Y.

Kang and C. T. Chen form National Taiwan University for simulation support. Work at JHU was supported by KAUST (Award # OSR2017-CRG6-3427.01) and the US Department of Energy (Award # DE-SC0009390 and SC0012670).

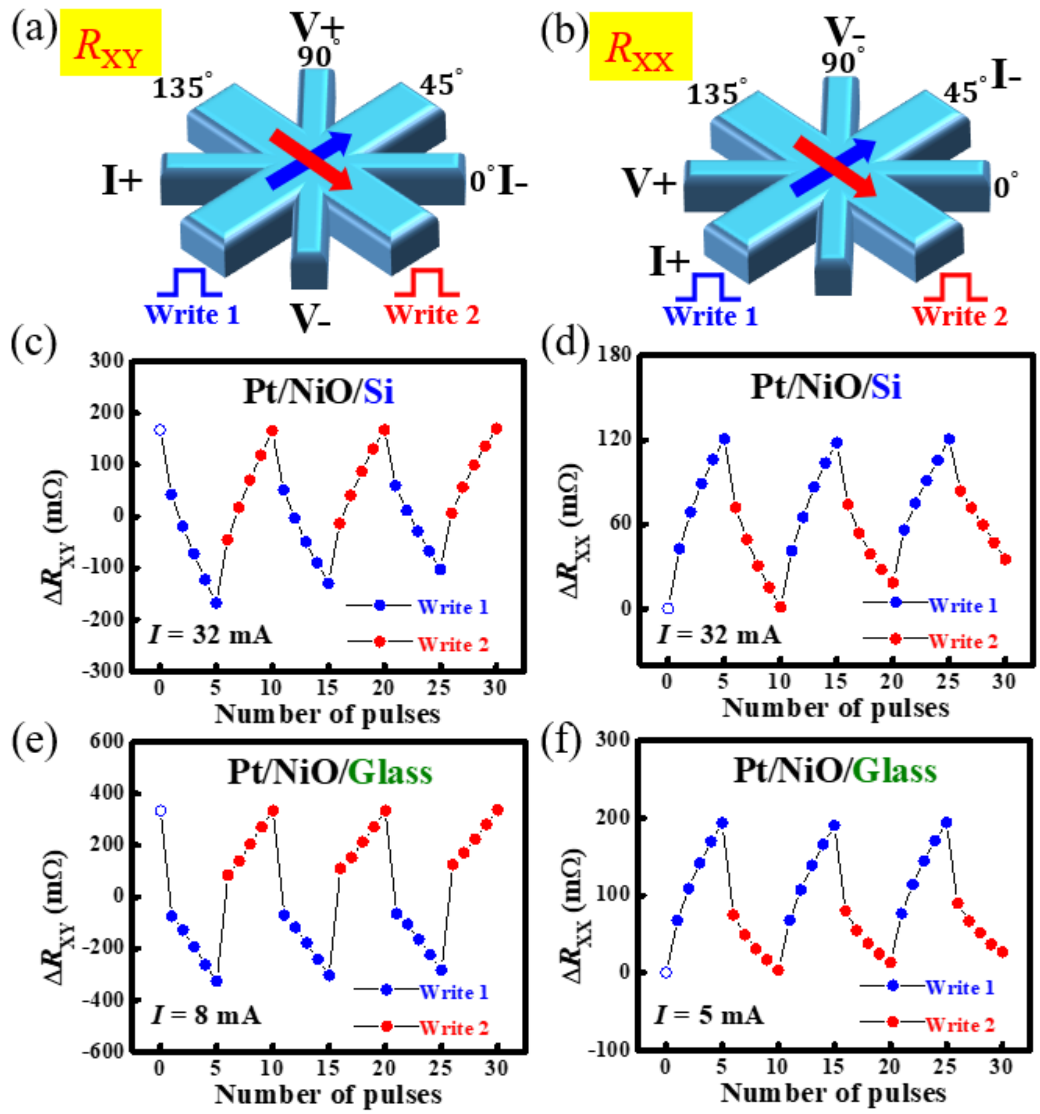

Fig. 1 Schematics of the 8-terminal patterned structure with the pulsed writing current along the 45° (write 1) and the 135° (write 2) lines for (a) planar Hall and (b) longitudinal resistance measurements. Relative changes of Hall resistance (ΔR_{XY}) in (c) Pt/NiO/Si and (e) Pt/NiO/Glass and relative change of longitudinal resistance (ΔR_{XX}) in (d) Pt/NiO/Si and (f) Pt/NiO/Glass, after applying 10-ms writing current pulses alternately along the 45° and the 135° lines.

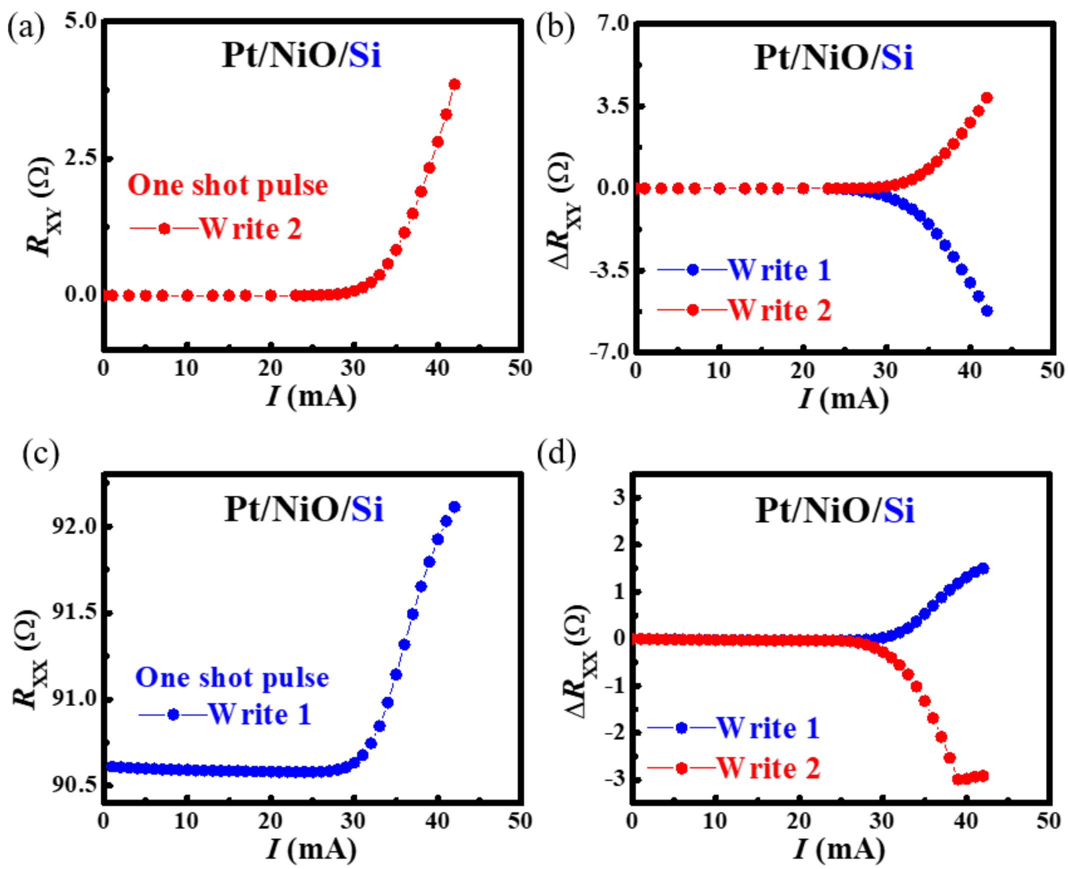

Fig. 2 (a) R_{XY} and (b) ΔR_{XY} in Pt/NiO/Si as a function of one-shot writing current pulses along the 45° (write 1) or the 135° (write 2) lines. (c) R_{XX} and (d) ΔR_{XX} in Pt/NiO/Si as a function of one-shot current pulse along the 45° (write 1) or the 135° (write 2) lines.

.

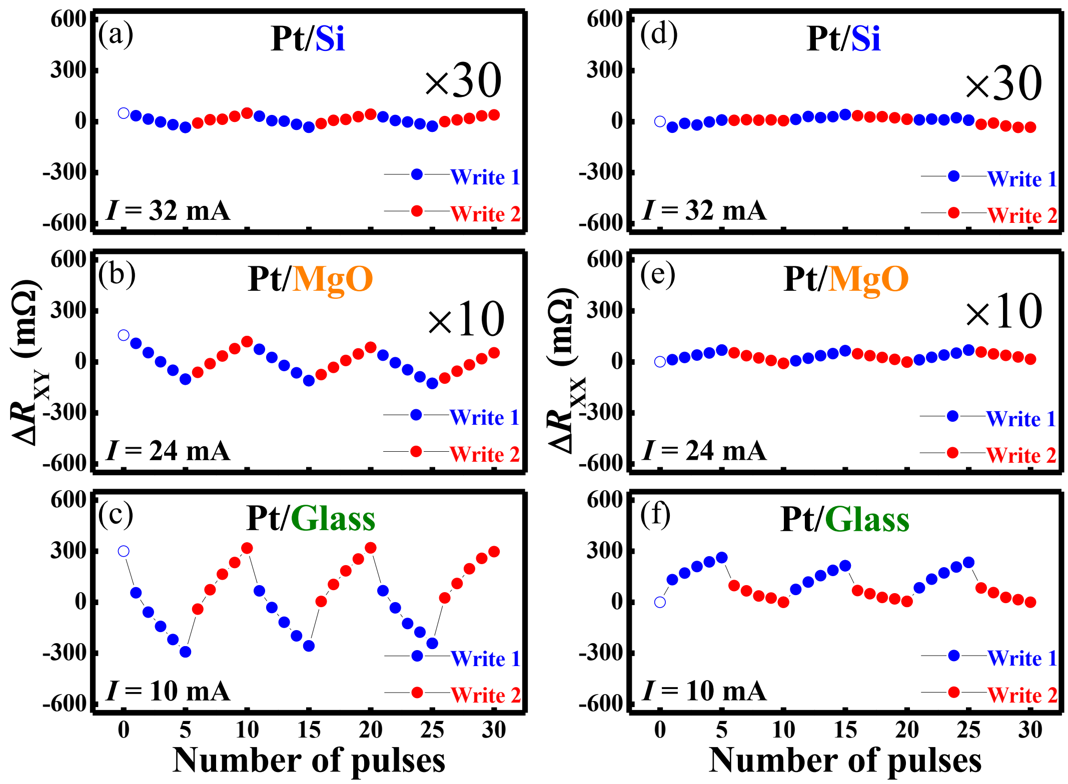

Fig. 3. The values of ΔR_{XY} and ΔR_{XY} after applying successive writing pulses current alternately along the 45° and the 135° lines for (a) Pt/Si, (b) Pt/MgO, and (c) Pt/glass; and for (d) Pt/Si, (e) Pt/MgO, and (f) Pt/glass, respectively, without any AF.

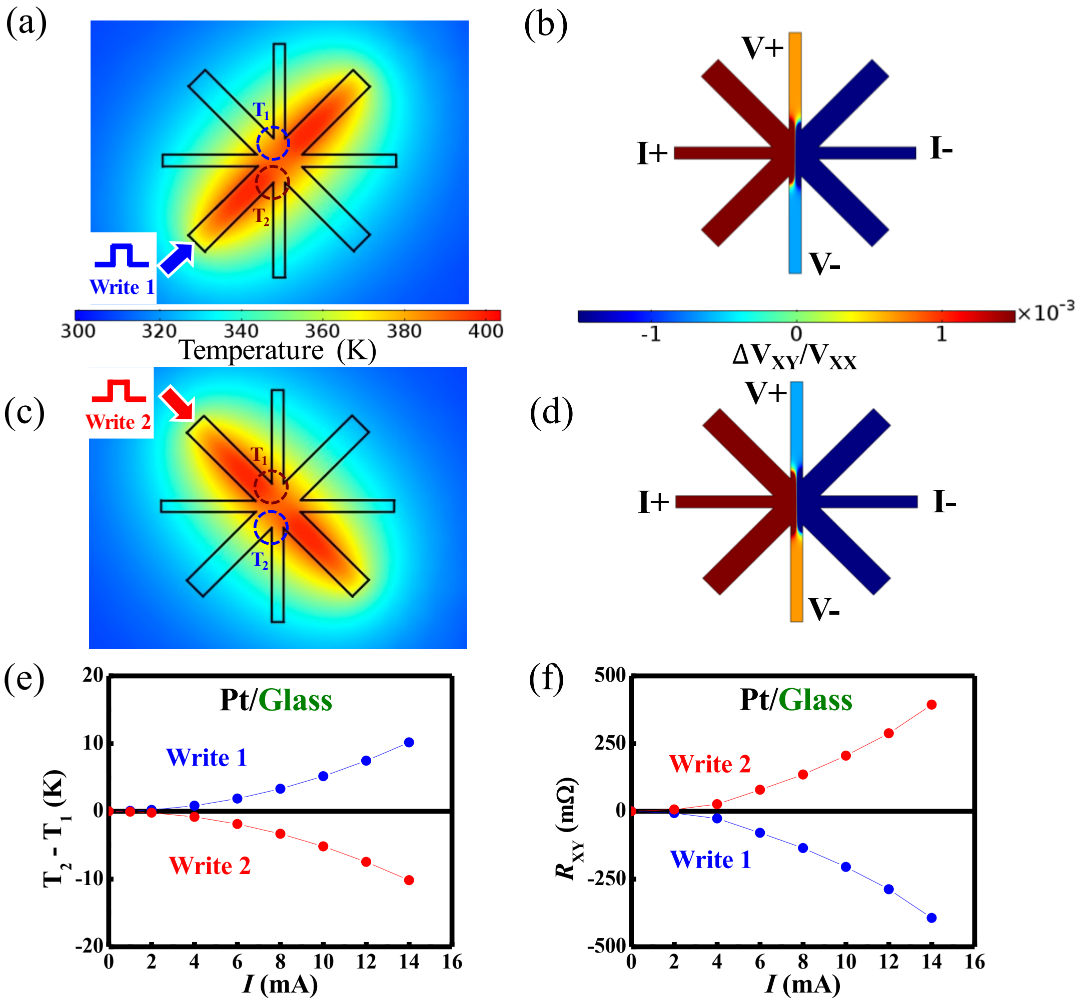

Fig. 4. Simulation of temperature distribution for the 8-terminal patterned Pt/glass structure after applying one-shot current of density 1.75 x 10^7 A/cm^2 along (a) 45° (write 1) and (c) 135° (write 2) lines. Simulation of Hall signal induced after one-shot writing current along (b) 45° (write 1) and (d) 135° (write 2) lines with relative Seebeck coefficient of 8 μV/K. (e) The temperature difference between T_1 and T_2 and (f) R_{XY} as a function of one-shot current pulse along 45° (write 1) and (c) 135° (write 2) lines.

Table. 1. Thermal conductivity of Si, MgO, and Glass [33]. Simulation of rising temperature in Pt (4 nm) on Si, MgO and glass and temperature difference between T_1 and T_2 in Fig. 4 (a), after applying one-shot writing current of density of 1.75 x 10^7 A/cm^2.

Substrate	**Thermal conductivity (W/mK)**	**T_1 (K)**	**T_2 (K)**	**ΔT (K)**
Silicon	131	301.25	301.36	0.11
MgO	30	304.92	305.38	0.46
Glass	1.38	383.64	393.78	10.14

*syhuang@phys.ntu.edu.tw

References

[1] E. B. Myers, D. C. Ralph, J. A. Katine, R. N. Louie, R. A. Buhrman, Science **285**, 5429 (1999), and D.C. Ralph, M.D. Stiles, J. Mag. Mag, Mater., **320** 1190 (2008).

[2] L. Liu, C. F. Pai, Y. Li, H. W. Tseng, D. C. Ralph, R. A. Buhrman, Science **336**, 6081 (2012).

[3] I. M. Miron, K. Garello, G. Gaudin, P. J. Zermatten, M. V. Costache, S. Auffret, S. Bandiera, B. Rodmacq, A. Schuhl, and P. Gambardella, Nature **476**, 189 (2011).

[4] L. Liu, O. J. Lee, T. J. Gudmundsen, D. C. Ralph, and R. A. Buhrman, Phys. Rev. Lett. **109**, 096602 (2012).

[5] G. Yu, P. Upadhyaya, Y. Fan, J. G. Alzate, W. Jiang, K. L. Wong, S. Takei, S. A. Bender, L. T. Chang, Y. Jiang, M. Lang, J. Tang, Y. Wang, Y. Tserkovnyak, P. K. Amiri, and K. L. Wang, Nat. Nanotechnol. **9**, 548 (2014).

[6] L. Youa, O. Leea, D. Bhowmika, D. Labanowskia, J. Honga, J. Bokora, and S. Salahuddin, Proc. Natl. Acad. Sci. U.S.A. **112**, 10310 (2015).

[7] Y. W. Oh, S. H. Chris Baek, Y. M. Kim, H. Y. Lee, K. D. Lee, C. G. Yang, E. S. Park, K. S. Lee, K. W. Kim, G. Go, J. R. Jeong, B. C. Min, H. W. Lee, K. J. Lee, and B. G. Park, Nat. Nanotechnol. **11**, 878 (2016).

[8] S. Fukami, C. Zhang, S. DuttaGupta, A. Kurenkov, and H. Ohno, Nat. Mater. **15**, 535 (2016).

[9] A. van den Brink, G. Vermijs, A. Solignac, J. Koo, J. T. Kohlhepp, H. J. Swagten, and B. Koopmans, Nat. Commun. **7**, 10854 (2016).

[10] Q. Ma, Y. Li, D. B. Gopman, Y. P. Kabanov, R. D. Shull, and C. L. Chien, Phys. Rev. Lett. **120**, 117703 (2018).

[11] S. C. Baek, V. P. Amin, Y. W. Oh, G. Go, S. J. Lee, G. H. Lee, K. J. Kim, M. D. Stiles, B. G. Park, and K. J. Lee, Nat. Mater. **17**, 509 (2018).

[12] T. C. Chuang, C. F. Pai, and S. Y. Huang, Phys. Rev. Applied **11**, 061005 (2019).

[13] P. Wadley, B. Howells, J. Železný, C. Andrews, V. Hills, R. P. Campion, V. Novák, K. Olejník, F. Maccherozzi, S. S. Dhesi, S. Y. Martin, T. Wagner, J. Wunderlich, F. Freimuth, Y. Mokrousov, J. Kuneš, J. S. Chauhan, M. J. Grzybowski, A. W. Rushforth, K. W. Edmonds, B. L. Gallagher, and T. Jungwirth, Science **351**, 587 (2016).

[14] S. Yu. Bodnar, L. Šmejkal, I. Turek, T. Jungwirth, O. Gomonay, J. Sinova, A. A. Sapozhnik, H.-J. Elmers, M. Kläui & M. Jourdan, Nat. Commun. **9**, 348 (2018).

[15] X. F. Zhou, J. Zhang, F. Li, X. Z. Chen, G. Y. Shi, Y. Z. Tan, Y. D. Gu, M. S. Saleem, H. Q. Wu, F. Pan, and C. Song, Phys. Rev. Applied **9**, 054028 (2018).

[16] X. Z. Chen, R. Zarzuela, J. Zhang, C. Song, X. F. Zhou, G. Y. Shi, F. Li, H. A. Zhou, W. J. Jiang, F. Pan, and Y. Tserkovnyak, Phys. Rev. Lett. **120**, 207204 (2018).

[17] T. Moriyama, K. Oda, T. Ohkochi, M. Kimata, and T. Ono, Sci. Rep. **8**, 14167 (2018).

[18] L. Baldrati, O. Gomonay, A. Ross, M. Filianina, R. Lebrun, R. Ramos, C. Leveille, T. Forrest, F. Maccherozzi, E. Saitoh, J. Sinova, and M. Kläui, arXiv:1810.11326v1.

[19] V. Baltz, A. Manchon, M. Tsoi, T. Moriyama, T. Ono, and Y. Tserkovnyak, Rev. Mod. Phys. **90**, 015005 (2018).

[20] J. Nogué, and I. K. Schuller, J. Mag. Mag, Mater., **192**, 203 (1999).

[21] G. R. Hoogeboom, A. Aqeel, T. Kuschel, T. T. M. Palstra, and B. J. van Wees, Appl. Phys. Lett. **111**, 052409 (2017).

[22] J. Fischer, O. Gomonay, R. Schlitz, K. Ganzhorn, N. Vlietstra, M. Althammer, H. Huebl, M. Opel, R. Gross, S. T. B. Goennenwein, and S. Geprägs, Phys. Rev. B **97**, 014417 (2018).

[23] L. Baldrati, A. Ross, T. Niizeki, C. Schneider, R. Ramos, J. Cramer, O. Gomonay, M. Filianina, T. Savchenko, D. Heinze, A. Kleibert, E. Saitoh, J. Sinova, and M. Kläui, Phys. Rev. B **98**, 024422 (2018).

[24] Yi-Jia Chen and Ssu-Yen Huang, Phys. Rev. Lett. **117**, 247201 (2016).

[25] T. C. Chuang, P. L. Su, P. H. Wu, and S. Y. Huang, Phys. Rev. B **96**, 174406 (2017).

[26] See Supplemental Material for more details on COMSOL simulations for 8 and 4 terminal devices, the time dependent Hall resistance with different substrates and normal metals, and the evolution between the saw-tooth and the step-like switching behaviors, which includes Refs. [27].

[27] G. A. Slack, J. Appl. Phys. **35**, 339 (1964).

[28] W. M. Haynes, CRC Handbook of Chemistry and Physics, 95th Edition (Oakville, CRC Press, 2014).

[29] M. Meinert, D. Graulich, and T. Matalla-Wagner, Phys. Rev. Appl. **9**, 064040 (2018).

[30] T. Matalla-Wagner, M.-F. Rath, D. Graulich, J.-M. Schmalhorst, G. Reiss, M. Meinert, arXiv:1903.12387.

[31] Y. Cheng, S. Yu, M. Zhu, J. Hwang, F. Yang, arXiv 1906.04694.

[32] P. Zhang, J. Finley, T. Safi, J. Han, and L. Liu, arXiv 1907.00314.

[33] S. Y. Huang, D. Qu, and C. L. Chien, Solid State Physics, Vol. 64 (Elsevier, 2013), pp. 53–82.